Improving PID-Control of AMB-Rotor System Design I: Optimization Strategy

Chunsheng Wei*
University of Duisburg-Essen
Duisburg, NRW, Germany

Dirk Söffker
University of Duisburg-Essen
Duisburg, NRW, Germany

Abstract

Most of the industial active magnetic bearings (AMBs) are controlled by PID-Controllers. Usually a time-consuming iterately procedure is involed to design those PID-Controllers. In this contribution an optimization strategy is developed to design a complex PID-Controller. Multi-Objective Genetic Algorithms (MOGAs) are employed as the core of the complex optimization procedure to be used. The results are studied. Core of this contribution is the development of the optimization strategy, especially the combination of frequency and time domain-based components as well as the strategy for complex PID-Controller design. For validation purposes, a comparison between simulation and experimental results are presented in part II of the contribution .

1 Introduction

Due to their advantages in comparison of conventional bearings, active magnetic bearings (AMB) have been applied to various rotor systems. For an AMB system, the inherent negative stiffness causes instability of the open loop of the system; therefore, a feedback control loop is employed to stabilize the rotor system. So the controller design becomes a central task for designing the AMB system. Different control methods are successfully applied to control magnetic bearing systems. The classical PID-Control methods [PRv+05] are widely used in AMB systems due to their structure and transparent design. An optimal method (LQ controller) [JP09, SB08] is used to obtain optimal (high performance) solution concerning control energy and control error. A drawback of these methods is that the robustness properties are not explicitly taken into account and that all states are needed to be used for feedback (therefore, an observer becomes necessary). Robust control methods (H_∞-controller [Wo11], μ-synthesis [MLA12]) are developed to cover up some drawbacks of LQ methods, focusing on both performance and robustness of the controlled system. However those methods result to high order controller which can cause implementation problems due to hardware limitations.

Most of industry AMB systems are controlled by PID-like controllers including also complex low-pass filter. Nowadays, rotor systems become more and more complex (because of higher energy density, higher speed, more complex rotor structure, etc.). A classic PID-Controller with only 3 parameters (K_P, T_i, and T_d) is overwhelmed to achieve various requirement, therefore a more complex controller structure is neccessary, e.g. PID-Controller with notch filter, lag-lead filter, and low-pass filter. This complicates the controller design and requires experience to tune controller parameters. The design procedure is hence iteratively and time-consuming. Motivated by this situation, an optimization procedure is developed and suggested in the contribution to design the controller parameters automatically.

This paper is organized as follows: In Section 2 the models of the rotor system and the magnetic bearing system are introduced. In Section 3 the controller design is focused. In Section 4 the detailed

*Contact Author Information: E-mail: Chunsheng.wei@uni-due.de; Address: University of Duisburg-Essen, Chair of Dynamics and Control, Lotharstr. 1-21, 47057 Duisburg, Germany; Phone: +49 (0) 203 / 379 - 15 80; Fax: +49 (0) 203 / 3 79 - 30 27

optimization strategy is presented, which is the core of this contribution. In Section 5, simulations are performed and results are compared for two selected controller candidates from pareto front. Finally, a summary is given in Section 6. In part II of the contribution, the experimental results are presented for validation.

2 Modeling

An AMB-rotor system includes the rotor system to be controlled as explained in part II of the contribution, sensors, analog-to-digital converters (AD-converters), controllers, digital-to-analog converters (DA-converters), amplifiers, and actuators. At first modeling of the rotor system will be discussed; secondly the model of the magnetic bearing system is given. The sensors are taken as proportional transfer elements of second order (PT2) with an eigenfrequency out of the sampling region of the system. Pulse-Width-Modulation (PWM) amplifiers are employed in the test-rig. Current control configuration is chosen, so the amplifiers can be modeled as part of actuators and treated by proportional behavior. The AD-converters and DA-converters are considered by constant gains, denoted by ADG and DAG, respectively.

2.1 Rotor System

The discretized model of the rotor (Figure 1) is modeled with 29 nodes and totally 116 DoFs (each node possesses 4 DoFs, i.e. translation and rotation in x- and y-plane). The equations of motion result to

$$\begin{aligned} \mathbf{M}\ddot{\mathbf{q}} + (\mathbf{D} + \Omega\mathbf{G})\dot{\mathbf{q}} + \mathbf{K}\mathbf{q} &= \mathbf{F}\mathbf{w}, \\ \mathbf{y} &= \mathbf{C}\mathbf{q}, \end{aligned} \tag{1}$$

with

$\mathbf{M}$:	Mass matrix,	$\mathbf{D}$:	Damping matrix (proportional damping $\mathbf{D} = \gamma\mathbf{K}$),
$\mathbf{G}$:	Gyroscopic matrix,	$\mathbf{K}$:	Stiffness matrix,
$\mathbf{F}$:	Input matrix,	$\mathbf{C}$:	Output matrix (corresponding to sensor nodes),
$\mathbf{y}$:	Measured nodes	$\mathbf{q}$:	Displacement vector, $\mathbf{q} = [\mathbf{q}_1^T, \mathbf{q}_2^T, \cdots, \mathbf{q}_{29}^T]^T$, $\mathbf{q}_i = [x_i, y_i, \alpha_i, \beta_i]^T$
Ω:	Rotational speed, and	$\mathbf{w}$:	Input force.

The equations of motion are transformed into a state-space representation using the state vector $\mathbf{x}_r = [\mathbf{q}^T, \dot{\mathbf{q}}^T]^T$ by

$$\begin{aligned} \dot{\mathbf{x}}_r &= \mathbf{A}_r\mathbf{x}_r + \mathbf{B}_r\mathbf{u}_r, \\ \mathbf{y}_r &= \mathbf{C}_r\mathbf{x}_r, \end{aligned} \tag{2}$$

where

$$\mathbf{A}_r = \begin{bmatrix} \mathbf{0} & \mathbf{I} \\ -\mathbf{M}^{-1}\mathbf{K} & -\mathbf{M}^{-1}(\mathbf{D} + \Omega\mathbf{G}) \end{bmatrix}, \quad \mathbf{B}_r = \begin{bmatrix} \mathbf{0} \\ \mathbf{M}^{-1}\mathbf{F} \end{bmatrix},$$

$$\mathbf{C}_r = \begin{bmatrix} \mathbf{C} & \mathbf{0} \end{bmatrix}, \quad \text{and} \quad \mathbf{y}_r = \mathbf{y},$$

with the system matrix $\mathbf{A}_r$ of order 232×232, the input matrix $\mathbf{B}_r$ of order 232×4, and the output matrix $\mathbf{C}_r$ of order 4×232.

The state-space model will be used for controller design. The eigenmodes of the rotor are shown in Figure 2. It is known that the eigenmodes and eigenfrequencies of a rotor system are speed dependent if gyroscopic effects are considered; the eigenmodes of the system in Figure 2 are displayed for the rotor at rest, consisting of the first four bending modes.

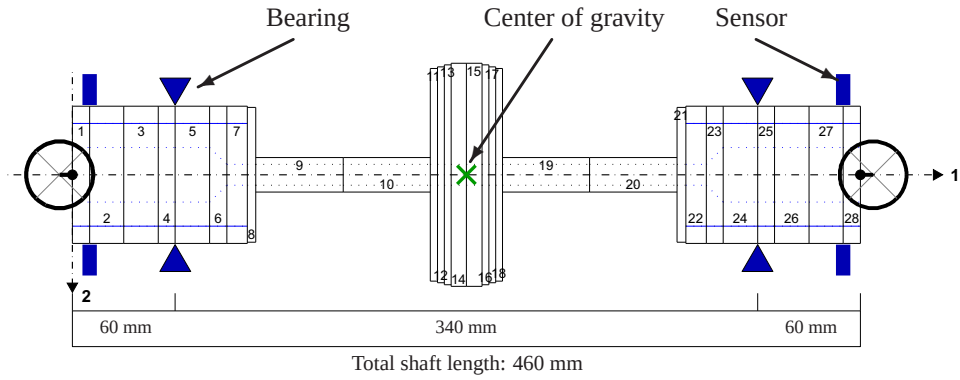

Figure 1: Discretized rotor model

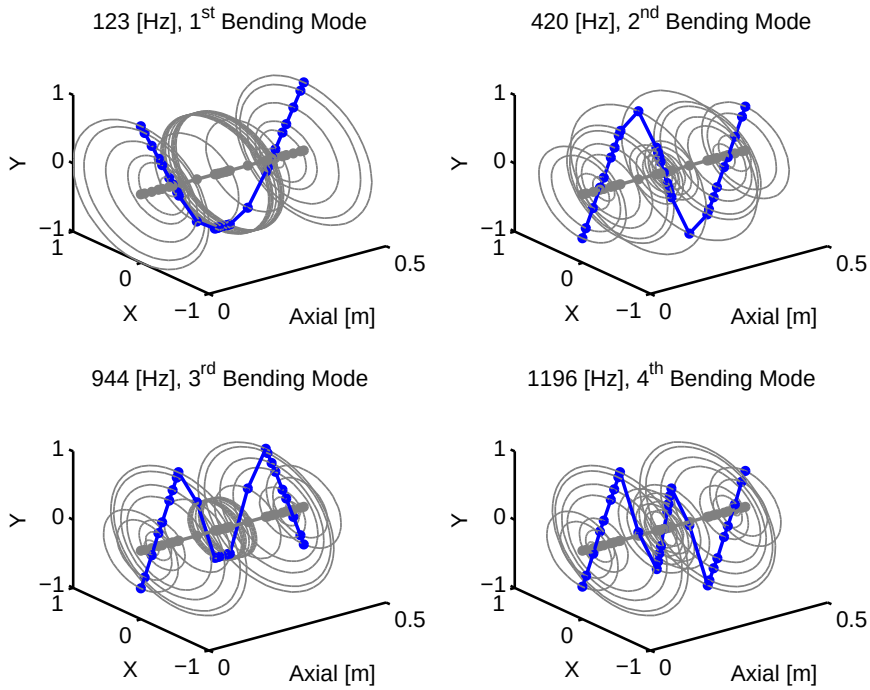

Figure 2: Eigenmodes of the rotor system

2.2 Magnetic Bearing Model

According to the available test-rig, the differential drive configuration as shown in Figure 3 is employed to linearize the force-current relation of the actuator. In order to achieve current control, an additional underlying current controller (P-Controller) is used to feedback the measured current of the magnet coils. The whole actuator system [SM09] including magnets, amplifiers, and the underlying current controllers, can be represented in state space form by

$$\begin{aligned} \dot{\mathbf{x}}_m &= \mathbf{A}_m\mathbf{x}_m + \mathbf{B}_m\mathbf{u}_m, \\ \mathbf{y}_m &= \mathbf{C}_m\mathbf{x}_m, \end{aligned} \tag{3}$$

with the displacement of the bearing nodes and the control current as inputs $\mathbf{u}_m$ of order 8×1, magnetic forces as outputs $\mathbf{y}_m$ of order 4×1, the state vector $\mathbf{x}_m$ of order 4×1, system matrix $\mathbf{A}_m$ of order 4×4, input matrix $\mathbf{B}_m$ of order 4×8, and outputs matrix $\mathbf{C}_m$ of order 4×4.

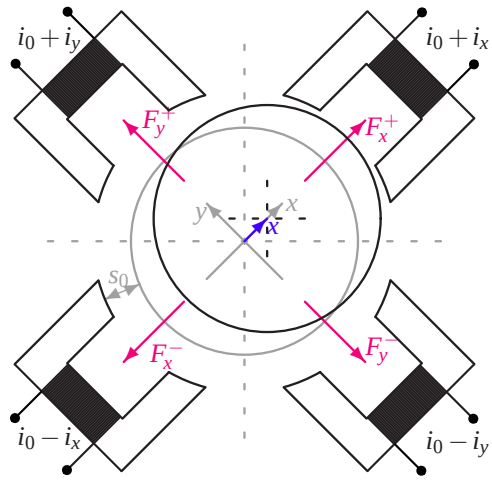

Figure 3: Actuator geometry (differential drive configuration)

2.3 Complete Model

Combining the sensor, the rotor, and the magnetic bearing models results to the complete plant model

$$\begin{aligned} \dot{\mathbf{x}} &= \mathbf{A}\mathbf{x} + \mathbf{B}\mathbf{u}, \\ \mathbf{y} &= \mathbf{C}\mathbf{x}, \end{aligned} \tag{4}$$

with the state vector $\mathbf{x} = [\mathbf{x}_s^T, \mathbf{x}_r^T, \mathbf{x}_m^T]^T$ ($\mathbf{x}_s^T$: sensor state vector of order 8).

The resulting plant possesses 244 states with 4 inputs and 4 outputs. The inputs of the plant are control currents and outputs of the sensors are considered as the outputs of the plant. Numerical parameters of the plant are given in Table 1.

In Figure 4 the bode diagram of the plant including sensors, rotor, magnetic bearings, AD-converters, DA-converters, and transformation matrices (which transform sensor coordinates to center of gravity coordinates and then back to bearing coordinates, detailed in the next Section) is shown. It can be seen that the parallel mode and tilting mode of the plant are perfect separated due to the symmetry of the rotor.

	Value		Value
Mass of the rotor [kg]	12.4	Length of the rotor [m]	0.46
Bearing stiffness k_s [N/m]	-2.8e6	Force/current factor k_i [N/A]	250
Air gap s_0 [m]	4.2e-4	Bias current [A]	5

Table 1: Numerical parameters of the system design

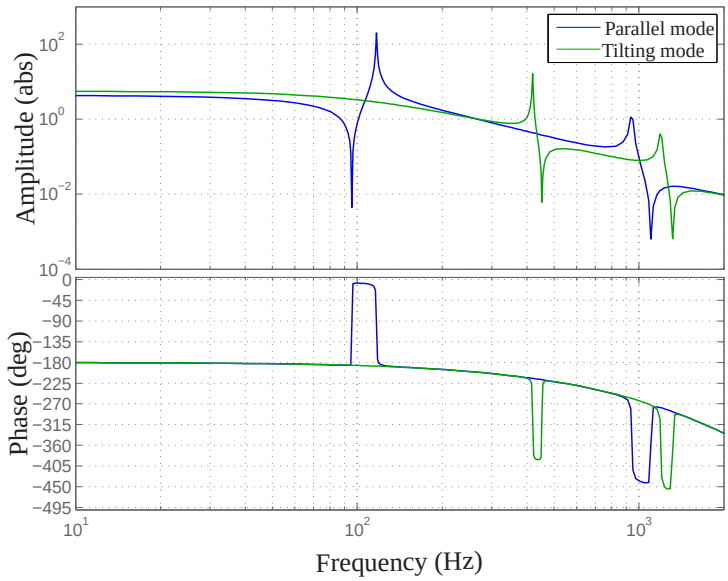

Figure 4: Bode diagram of the plant

3 Controller Design

In this Section a so called 'Trans-Tilt' (Translation and Tilting mode) PID-Controller design for the AMB-rotor system is briefly described. Since the rotor is quite elastic, the first 4 bending modes have to be considered by the controller design.

Firstly, the sensor-coordinates are transformed into the center of gravity coordinates using a transformation matrix, resulting in x-plane as

$$\begin{aligned} x_\mathrm{c} &= \frac{1}{2}(x_\mathrm{l} + x_\mathrm{r}), \\ \beta &= (x_\mathrm{r} - x_\mathrm{l})/\mathrm{l_s}, \end{aligned} \tag{5}$$

or

$$\begin{bmatrix} x_\mathrm{c} \\ \beta \end{bmatrix} = \underbrace{\begin{bmatrix} \frac{1}{2} & \frac{1}{2} \\ -\frac{1}{\mathrm{l_s}} & \frac{1}{\mathrm{l_s}} \end{bmatrix}}_{\text{Transformation matrix}} \begin{bmatrix} x_\mathrm{l} \\ x_\mathrm{r} \end{bmatrix}. \tag{6}$$

The indexes l, r, and c denote left sensor node, right sensor node, and rotor midspan node, respectively. The distance of two sensor nodes is denoted as l_s.

The transformation allows the decoupling of 'parallel' modes and 'tilting' modes of the rotor. An advantage obtained by this transformation is that the controller design can be achieved separately for parallel mode and the tilting mode.

For parallel and tilting mode control, the same controller structure is used. The PID-Controller consisting of 2 parts (PDT_1 with filters and an integrator) is introduced. The first part is limited to be an order of 7 due to hardware requirement. The first part of the PID-Controller can be written as,

$$\begin{aligned} K_{\mathrm{PD}} &= K_{\mathrm{P}} \underbrace{\frac{\frac{s}{\omega_{\mathrm{n0}}}+1}{\frac{s}{\omega_{\mathrm{d0}}}+1}}_{\mathrm{PDT}_1} \underbrace{\frac{(\frac{s}{\omega_{\mathrm{n1}}})^2+2\xi_{n1}\frac{s}{\omega_{\mathrm{n1}}}+1}{(\frac{s}{\omega_{\mathrm{d1}}})^2+2\xi_{\mathrm{d1}}\frac{s}{\omega_{\mathrm{d1}}}+1}}_{\text{filter 1 } (\mathrm{F}_1)} \underbrace{\frac{(\frac{s}{\omega_{\mathrm{n2}}})^2+2\xi_{n2}\frac{s}{\omega_{\mathrm{n2}}}+1}{(\frac{s}{\omega_{\mathrm{d2}}})^2+2\xi_{\mathrm{d2}}\frac{s}{\omega_{\mathrm{d2}}}+1}}_{\text{filter 2 } (\mathrm{F}_2)} \underbrace{\frac{(\frac{s}{\omega_{\mathrm{n3}}})^2+2\xi_{n3}\frac{s}{\omega_{\mathrm{n3}}}+1}{(\frac{s}{\omega_{\mathrm{d3}}})^2+2\xi_{\mathrm{d3}}\frac{s}{\omega_{\mathrm{d3}}}+1}}_{\text{filter 3 } (\mathrm{F}_3)}, \\ &= \mathrm{PDT}_1 \cdot \mathrm{F}_1\,\mathrm{F}_2\,\mathrm{F}_3. \end{aligned} \tag{7}$$

It can be seen that the controller uses 15 parameters: K_{P}, ω_{n0}, ω_{d0}, ω_{n1}, ξ_{n1}, ω_{d1}, ξ_{d1}, ω_{n2}, ξ_{n2}, ω_{d2}, ξ_{d2}, ω_{n3}, ξ_{n3}, ω_{d3}, and ξ_{d3}.

Furthermore, adding an integrator term to the controller K_{PD} gives the final PID-Controller structure to be used as

$$K = K_{\mathrm{PD}} + \frac{K_{\mathrm{I}}}{s} = \mathrm{PDT}_1 \cdot \mathrm{F}_1\,\mathrm{F}_2\,\mathrm{F}_3 + \frac{K_{\mathrm{I}}}{s}. \tag{8}$$

For the parallel and tilting mode control, two PID-Controllers with the same controller structure as mentioned above are needed. The overall system considering x- and y-plane motions requires 4 PID-Controllers, i.e. two controllers (parallel and tilting mode) for each plane.

Finally, the control current (as controller output) has to be transformed back into bearing-coordinates to be fed into the cooresponding actuators as,

$$\begin{bmatrix} i_{\mathrm{l}} \\ i_{\mathrm{r}} \end{bmatrix} = \underbrace{\begin{bmatrix} 1 & -1 \\ 1 & 1 \end{bmatrix}}_{\substack{\text{Transformation} \\ \text{matrix}}} \begin{bmatrix} i_{\mathrm{p}} \\ i_{\mathrm{t}} \end{bmatrix}. \tag{9}$$

The indexes p and t denote the parallel and tilting mode, respectively.

The parameters of two controllers (parallel and tilting mode) will be determined and optimized in the next Section.

4 Optimization Strategy

As described in last Section, totally 30 parameters from the parallel and tilting mode controller have to be choosen. The hand-tuning procedure can be time-consuming, especially if various (competing) criteria has to be considered.

The solution idea of this contribution is to use the design parameters (controller parameters) of the design process (AMB-rotor system) as parameters to be optimized and to evaluate the resulting system behavior with given criteria, taking into account the overall system requirements. It is clear that this is a multi-objective optimization problem. The optimization task will be solved by using MOGAs. Different MOGAs and MOEAs (Multi-Objective Evolutionary Algorithms) are available for solving such optimization problem. Ceollo [Coe98, Coe06] gives a survey about

evolutionary-based optimization techniques. In papers [Coe98, Coe06] the most well-known MOGAs and MOEAs are introduced and related advantages and disadvantages are analysed. Fleming and Purshouse [FP02] summarize evolutionary algorithms with the focus on the application of control engineering. In [Deb01] a detailed introduction of different evolutionary algorithms is given.

Among those optimization algorithms, NSGA-II (Nondominated Sorting Genetic Algorithm II), which was introduced in the paper [DPAM02] by Deb et al., becomes very popular due to its computational efficiency. The optimization results of this contribution are obtained by using the MOGAs (a variant of NSGA-II) from the global optimization toolbox in Matlab®.

4.1 Evaluation of Fitness Functions

Diverse criteria have to be formulated as objectives (also called fitness functions). Some of these criteria can be considered as constraints. This is a crucial point to use the MOGA. The optimization problem can be solved quite efficient with well-defined fitness functions, on the contrary the optimization can be failed due to non-convengence.

An another challenge arising from the control problem is the requirement for stability of the closed-loop. The stability requirements of the closed-loop of the AMB-rotor system can be treated either as a constraint during the optimization process or as an objective to maximize the stability degree d as

$$d = 0 - \max\{\Re(\lambda_i)\}, \quad i = 1,2...n,$$

with $\Re(\lambda_i)$ denoting the real part of the i-th eigenvalue and n denotes the number of the eigenvalue of the linear system.

This contribution presents a strategy for a hierarchical evaluation of the fitness functions for MOEAs and MOGAs. With this strategy, the optimizer tries to shift the candidates to the stable region of the closed-loop of the AMB-rotor system in the beginning period of the optimization process. Once this step is successful, the other objectives (including time and frequency domain criteria/performance ratios) become available to be optimized. There are two advantages following this strategy:

1. The optimization process is accelerated, since more feasible (stable) candidates will be found (if possible) in the beginning period of the optimization process for further optimization.

2. The probability that the optimization process will converge, increases.

It should be noted that a convergence can in principle not be guaranteed for those MOEAs and MOGAs due to their randomized character (if the feasible region is isolated (too small) in the defined search space). Certainly no global optimum even local optimum is guaranteed in principle for each objective.

In the following, the recommended evaluation strategy of the fitness functions is given in detail. Firstly, the fitness functions to be considered in the optimization of controlling AMB-rotor system are given. Totally five objectives are formulated as fitness functions. The maximal singular value of the sensitivity function $\sigma(S_{\mathrm{pt}})$ is treated as the first objective. It is defined as the larger one of the maximal singular value of parallel and tilting mode (see Section 3) sensitivity funcion (S_{p} and S_{t}), i.e.

$$F_1 = \sigma(S_{\mathrm{pt}}) = \max\{\sigma(S_{\mathrm{p}}), \sigma(S_{\mathrm{t}})\}.$$

The damping ratio of the eigenvalue in the frequency region [0..300] Hz and (300..1000] Hz are considered separately as two objectives, which are denoted as $D_{[0-300]}$ and $D_{(300-1000]}$. The first frequency region shall include the rigid body modes and the first bending mode. Since the

optimization goal is to minimize the fitness functions, the inverse damping ratio is defined as fitness function by

$$F_2 = D\text{inv}_{[0-300]} = \frac{1}{D_{[0-300]}} \quad \text{and}$$
$$F_3 = D\text{inv}_{(300-1000]} = \frac{1}{D_{(300-1000]}}.$$

These three fitness functions mentioned above are related to the frequency domain performance. For controlling AMB-rotor system, the time domain performance also has to be considered. Hereby, the overshoot A_{os} and the settling time t_{st} of the step response of the AMB-rotor system are taken into account; So two fitness functions cooresponding to the time domain performance,

$$F_4 = A_{\text{os}} \quad \text{and}$$
$$F_5 = t_{\text{st}}$$

are used.

The 5 fitness functions are evaluated with the strategy mentioned above for each individual in current population as follows:

Step I: The sensitivity **S** and complementary-sensitivity **T** function matrix are calculated, as well as their eigenvalues λ_i. If the closed-loop is stable, the procedure continues with step II, otherwise

$$F_1..F_5 = \max\{\Re(\lambda_i)\} + \text{constant A}$$

is used to evaluate the fitness functions.

Step II: The maximal singular value of the sensitivity functions for the parallel and tilting mode (which can be directly obtained from **S**) are evaluated and the singular values of the sensitivity function $\sigma(S_{\text{pt}})$ is defined. The inverse damping ratio of the eigenvalues is determined. Calculating the step response of the closed-loop gives the overshoot A_{os} and the settling time t_{st}. If the values of $\sigma(S_{\text{pt}})$, $D\text{inv}_{[0-300]}$, $D\text{inv}_{(300-1000]}$, A_{os} and t_{st} are not larger than a special suitable choosen number, the procedure continues and goes to step III, otherwise

$$F_1..F_5 = \max\{\Re(\lambda_i)\} + \text{constant B}$$

is used.

Step III: If the conditions

$$\sigma(S_{\text{pt}}) \leq 50, \quad D\text{inv}_{[0-300]} \leq 100, \quad \text{and} \quad A_{\text{os}} \leq 1000$$

are fullfilled, the objective functions are defined as

$$
\begin{aligned}
F_1 &= \sigma(S_{\mathrm{pt}}),\\
F_2 &= \begin{cases} D\mathrm{inv}_{[0-300]} & \text{if } D\mathrm{inv}_{[0-300]} \geq 2,\\ 2 & \text{if } D\mathrm{inv}_{[0-300]} < 2, \end{cases}\\
F_3 &= \begin{cases} D\mathrm{inv}_{(300-1000]} & \text{if } D\mathrm{inv}_{(300-1000]} \geq 20,\\ 20 & \text{if } D\mathrm{inv}_{(300-1000]} < 20, \end{cases}\\
F_4 &= \begin{cases} A_{\mathrm{os}} & \text{if } A_{\mathrm{os}} \geq 100,\\ 100 & \text{if } A_{\mathrm{os}} < 100, \end{cases} \quad \text{and}\\
F_5 &= \begin{cases} t_{\mathrm{st}} & \text{if } t_{\mathrm{st}} \geq 0.3,\\ 0.3 & \text{if } t_{\mathrm{st}} < 0.3, \end{cases}
\end{aligned}
\tag{10}
$$

otherwise

$$F_1..F_5 = \max\{\Re(\lambda_i)\} + \text{constant C}$$

is used.

It should be mentioned that "optimal" values are defined for the fitness functions $F_2..F_5$. If the fitness function reaches the related "optimal" value, then this fitness function does not need to be considered in the optimization process, therefore the optimizer focuses only on the other objectives. This again accelerates the optimization process. The optimal values of the fitness functions are given in Table 2.

Objective parameter	"Optimal" value	Description
$D\mathrm{inv}_{[0-300]}$	2 (= 50% Damping ratio)	Inverse damping ratio
$D\mathrm{inv}_{(300-1000]}$	20 (= 5% Damping ratio)	Inverse damping ratio
A_{os} [%]	100	Overshoot
t_{st} [sec]	0.3	Settling time

Table 2: Defined optimal values of the fitness functions

The search space of the controller parameters are given in Table 3. It should be noticed that only the part of the controller K_{PD} is considered for optimization. The integrator gain is determined by

$$K_{\mathrm{I}} = \mathrm{DCgain}(K_{\mathrm{PD}}) \cdot 2\pi \cdot 1$$

and the whole PID-Controller (Equation 8) is used to evaluate the fitness functions. The test-rig is designed to work with a maximal rotational speed of 15000 rpm, thus the rotor model with the rotational speed of 15000 rpm is employed for the controller design and optimization.

4.2 Optimization Results

The optimization results are shown in Figure 5. Each point from the Pareto front (see Figure 5 respresents an optimal solution, which is not dominated from other candidates. The upper right and lower left plots show that the fitness function $\sigma(S_{\mathrm{pt}})$ is competing with overshoot A_{os} as well as inverse damping ratio $D\mathrm{inv}_{(300-1000]}$, i.e. minimizing the max. singular value $\sigma(S_{\mathrm{pt}})$ can only be

		K_P	ω_{n0}	ω_{d0}	ω_{n1}	ξ_{n1}	ω_{d1}	ξ_{d1}	
Parallel mode	Lower bound	9e3	50	100	100	0.05	80	0.05	
	Upper bound	3e4	150	2e3	1e3	1.00	1e3	1.00	
Tilting mode	Lower bound	1.5e3	60	100	100	0.05	100	0.05	
	Upper bound	4e3	180	2e3	1e3	1.00	1e3	1.00	
		ω_{n2}	ξ_{n2}	ω_{d2}	ξ_{d2}	ω_{n3}	ξ_{n3}	ω_{d3}	ξ_{d3}
Parallel mode	Lower bound	100	0.05	100	0.05	300	0.05	300	0.05
	Upper bound	1e3	1.00	1e3	1.00	1e3	1.00	1e3	1.00
Tilting mode	Lower bound	150	0.05	150	0.05	300	0.05	300	0.05
	Upper bound	1e3	1.00	1e3	1.00	1e3	1.00	1e3	1.00

Table 3: Search space of controller parameters

achieved with increasing the overshoot A_{os} and decreasing the damping ratio of the eigenvalues in the frequency region (300..1000] Hz. The settling time t_{st} reaches the defined optimal value (see the lower right plot).

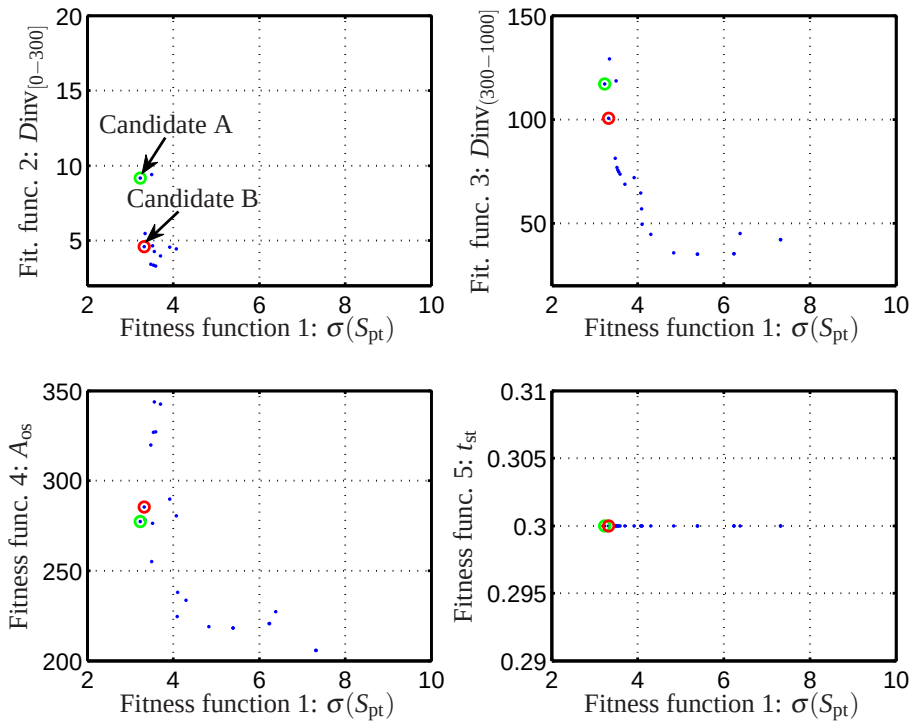

Figure 5: Pareto front

Two candidates (A and B) from the pareto front with the smallest max. singular value $\sigma(S_{pt})$ are selected for further simulation. The optimized objective values are given in Table 4. The resulting

Objective	Candidate A	Candidate B
Sinuglar value $\sigma(S_{pt})$	3.23	3.32
Damping ratio [0..300] Hz	11%	21%
Damping ratio (300..1e3] Hz	0.85%	0.99%
Overshoot A_{os}	277%	285%
Settling time t_{st}	0.3	0.3

Table 4: Objective value of selected candidates

maximal singluar values of candidates A and B are corresponding to zone B according to the ISO Stardard 14839-3. All eigenmodes of the closed-loop with controller candidate B in the frequency region [0..300] Hz are well damped. In the next Section the detailed simulation results will be presented.

It should be noted that the candidate has to be carefully selected from the pareto front. The optimizer tries to present all nondominated solutions based on the defined fitness functions, consequently, some outlier points are also found by the optimizer in order to form the whole pareto front. However, those points are usually unacceptable for example due to known realization problems.

5 Simulation Results

In the last Section, two (example) candidates are selected for simulation and will be implemented. In this Section the simulation results of the both candidates are given and compared.

		K_P	ω_{n0}	ω_{d0}	ω_{n1}	ξ_{n1}	ω_{d1}	ξ_{d1}	
Parallel	Cand. A	1.84e4	137	1.10e3	412	0.40	486	0.56	
mode	Cand. B	1.25e4	86	1.47e3	182	0.48	178	0.65	
Tilting	Cand. A	2.10e3	119	808	787	0.35	565	0.67	
mode	Cand. B	2.08e3	115	683	343	0.71	285	0.72	
		ω_{n2}	ξ_{n2}	ω_{d2}	ξ_{d2}	ω_{n3}	ξ_{n3}	ω_{d3}	ξ_{d3}
Parallel	Cand. A	622	0.38	464	0.46	667	0.68	652	0.81
mode	Cand. B	390	0.57	328	0.68	935	0.63	639	0.40
Tilting	Cand. A	828	0.75	657	0.70	718	0.51	768	0.56
mode	Cand. B	586	0.68	452	0.59	639	0.51	548	0.39

Table 5: Parameters of selected controller candidates

The corresponding controller parameters of selected candidates are summerized in Table 5. In Figure 6 the bode diagram of the controllers (including parallel and tilting mode controller) of both candidates is shown. The Parallel mode controller of candidate A has a larger P-part (K_P) compared with the one of candicate B. The tilting mode controllers are similar at low frequencies but differ from each other at high frequencies.

In Figure 7 the pole-zero map of the closed-loop is shown. It can be seen that the eigenmodes up to the first bending mode are well damped for both candidates. The first bending mode are even damped with more than 30% damping ratio.

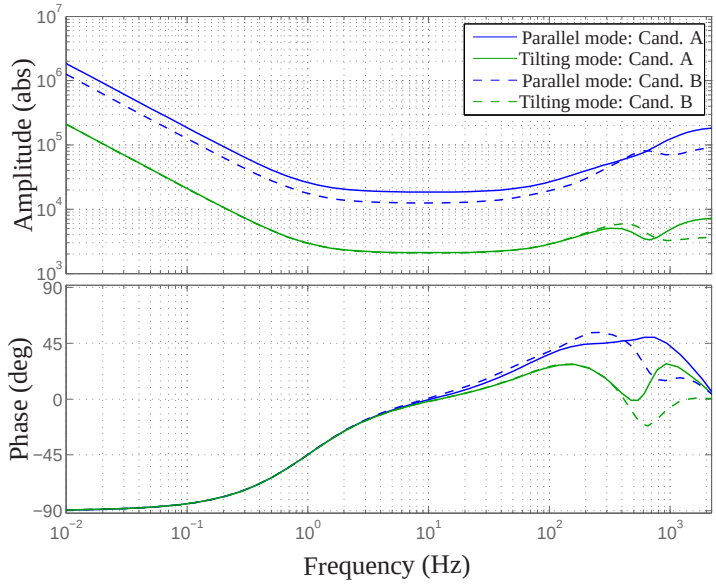

Figure 6: Bode diagram of selected controller candidates

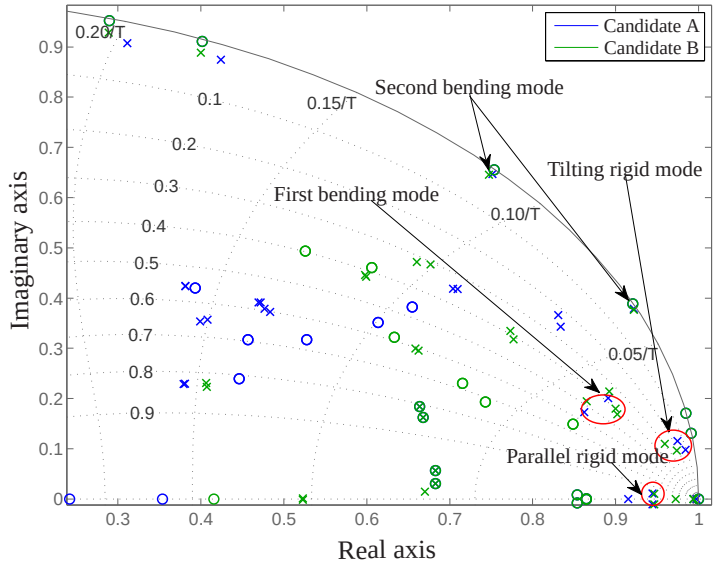

Figure 7: Pole-zero map of the closed-loop with the rotor at the rotational speed of 15000 rpm

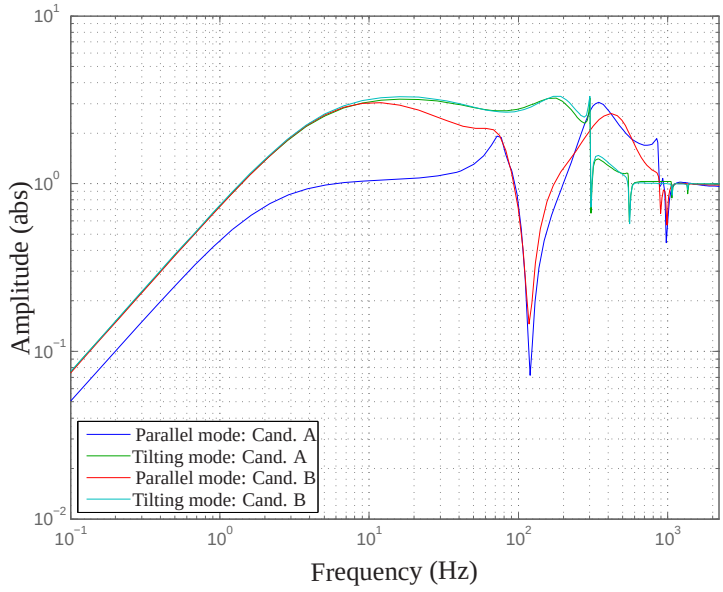

Figure 8: Singular values of the closed-loop with the rotor model at the rotational speed of 15000 rpm

The singular values for parallel and tilting mode of both candidates are illustrated in Figure 8. For the parallel mode large differences occur at low frequencies. The candidate A has a singular value only about 30% of the one of candidate B in the frequency region [2..30] Hz. For the tilting mode there is no remarkable difference.

The step response behavior is presented in Figure 9. The parallel mode of candidate A is superior over the one of candidate B with respect to the overshoot of the step response, however the result is quite similar for tilting mode.

The results above are determined with the rotor model at the rotational speed of 15000 rpm. In oder to ensure the stability and performance for the system when the rotor is at rest, simulations are neccessarily to be carried out. The simulation results (including the results with the rotor at rest) are summarized in Table 6. The performance of the system has no noticeable change due to rotation.

6 Summary

This paper presents an optimization approach by using multi-objective genetic algorithms for fast and optimal parameter design of a complex PID-Controller with respect to given requirements formuled in time and frequency domain. The challenges by using MOGAs/MOEAs are discussed and a corresponding evaluation strategy is suggested. The simulation results show that a PID-Controller of complex structure can be obtained/optimized by using MOGAs with the suggested evaluation strategy considering various criteria, limitations, and performance aspects.

For validation purpose, the obtained controllers are implemented for experiments. Experimental tests are performed and the results will be discussed in part II titled "*Improving PID-Control of AMB-rotor System II: Experimental Results*".

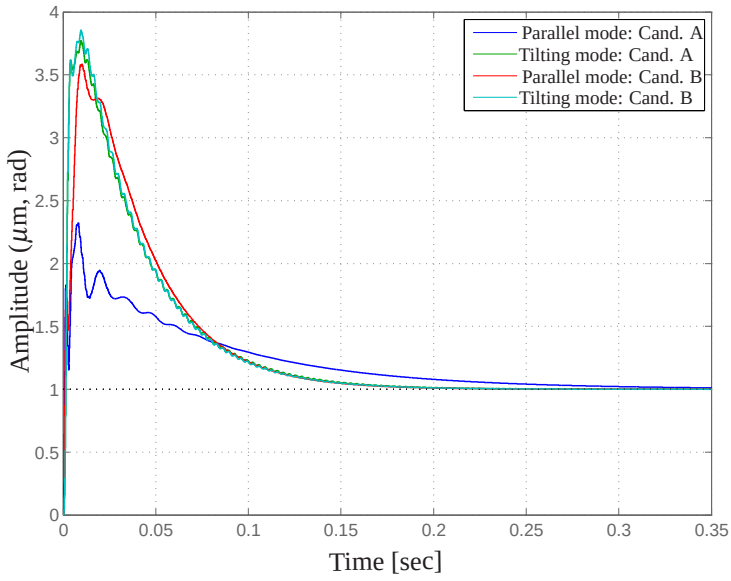

Figure 9: Step response of the closed-loop with the rotor model at the rotational speed of 15000 rpm

		Candidate A		Candidate B	
		0 rpm	1.5e4 rpm	0 rpm	1.5e4 rpm
Parallel mode	Max. sinuglar value	3.08	3.23	3.05	3.32
	Overshoot A_{os}	138%	132%	263%	258%
	Settling time t_{st}	0.28	0.28	0.15	0.15%
Tilting mode	Max. sinuglar value	3.3	3.25	3.37	3.34
	Overshoot A_{os}	275%	277%	283%	285%
	Settling time t_{st}	0.15	0.15	0.15	0.15%
Damping ratio	[0..300] Hz	13.2%	10.9%	25.4%	21.7%
	(300..1000] Hz	1.6%	0.85%	2.2%	0.99%

Table 6: Objective value of the selected candidates for rotational speed of 0 and 15000 rpm

References

[Coe98] Carlos A. Coello. A comprehensive survey of evolutionary-based multiobjective optimization techniques. *Knowledge and Information Systems*, 1:269–308, 1998.

[Coe06] Carlos A. Coello. Evolutionary multi-objective optimization: A historical view of the field. *IEEE Computational Intelligence Magazine*, pages 28–36, 2006.

[Deb01] K. Deb. *Multi-Objective Optimization using Evolutionary Algorithms*. Wiley-Interscience Series in Systems and Optimization. John Wiley & Sons, Chichester, 2001.

[DPAM02] K. Deb, A. Pratap, S. Agarwal, and T. Meyarivan. A fast and elitist multiobjective genetic algorithm: Nsga-ii. *IEEE Transactions on Evolutionary Computation*, 6(2):182–197, 2002.

[FP02] P.J. Fleming and R.C. Purshouse. Evolutionary algorithms in control system engineering: a survey.

Control Engineering Practice, Vol, 10:1223–1241, 2002.

[JP09] Rafał Piotr Jastrzębski and Riku Pöllönen. Centralized optimal position control for active magnetic bearings: comparison with decentralized control. *Electrical Engineering*, 91(2):101–114, 2009.

[MLA12] Simon E. Mushi, Zongli Lin, and Paul E. Allaire. Design, construction, and modeling of a flexible rotor active magnetic bearing test rig. *IEEE/ASME Transactions on Mechatronics*, PP(99):1–13, 2012.

[PRv+05] B Polajžer, J Ritonja, G Štumberger, D Dolinar, and J P Lecointe. Decentralized pi/pd position control for active magnetic bearings. *Electrical Engineering*, 89(1):53–59, 2005.

[SB08] Chip Rinaldi Sabirin and Andreas Binder. Rotor levitation by active magnetic bearing using digital state controller. In *Proceedings of 13th Int. Power Electronics and Motion Control Conf. (EPE-PEMC)*, pages 1625–1632. IEEE, September 2008.

[SM09] Gerhard Schweitzer and Eric H Maslen, editors. *Magnetic Bearings: Theory, Design, and Application to Rotating Machinery*. Springer Berlin Heidelberg, 2009.

[Wo11] Chunsheng Wei and Dirk Söffker. Optimal control of a flexible rotor by using magnetic bearing. In R. Markert, editor, *Proceedings of 9th Int. Conf. on Vibrations in Rotating Machines (SIRM 2011)*. Technische Universität Darmstadt, February 2011. Paper-ID: 49.